Continuous Cold-Atom Inertial Sensor with 1 nrad/sec Rotation Stability

I. Dutta, D. Savoie, B. Fang, B. Venon, C. l. Garrido Alzar, R. Geiger, A. Landragin

HAL Id: hal-01321643
https://hal.sorbonne-universite.fr/hal-01321643

Submitted on 20 Aug 2023

Continuous Cold-Atom Inertial Sensor with 1 nrad/sec Rotation Stability

I. Dutta, D. Savoie, B. Fang, B. Venon, C. L. Garrido Alzar, R. Geiger,[*] and A. Landragin[†]

LNE-SYRTE, Observatoire de Paris, PSL Research University, CNRS, Sorbonne Universités,
UPMC Univ. Paris 06, 61 avenue de l'Observatoire, 75014 Paris, France
(Received 19 January 2016; published 6 May 2016)

We report the operation of a cold-atom inertial sensor which continuously captures the rotation signal. Using a joint interrogation scheme, where we simultaneously prepare a cold-atom source and operate an atom interferometer (AI), enables us to eliminate the dead times. We show that such continuous operation improves the short-term sensitivity of AIs, and demonstrate a rotation sensitivity of $100 \text{ nrad/sec}/\sqrt{\text{Hz}}$ in a cold-atom gyroscope of 11 cm^2 Sagnac area. We also demonstrate a rotation stability of 1 nrad/sec at 10^4 sec of integration time, which represents the state of the art for atomic gyroscopes. The continuous operation of cold-atom inertial sensors will lead to large area AIs at their full sensitivity potential, determined by the quantum noise limit.

Over the past two decades, important progress in cold-atom physics has established atom interferometry as a unique tool for precision measurements of time and frequency and of gravito-inertial effects. Atom interferometry addresses various applications ranging from precision measurements of fundamental constants [1,2] to inertial navigation [3–5] to geophysics and geodesy [6–9], and has been proposed for gravitational wave detection [10,11]. New techniques are being developed to improve the potential of atom interferometers (AIs), such as large momentum transfer beam splitters [12,13], long interrogation times in tall vacuum chambers [14], microgravity platforms [4,15], or operation of AIs with ultracold atomic sources [16]. Advanced detection and atom preparation methods have, moreover, been proposed and demonstrated to go beyond the quantum projection noise in AIs [17,18]. However, benefiting from these new techniques to fully exploit the potential of AIs requires handling the problem of dead times between successive measurements occurring in cold-atom sensors.

Dead times in AIs originate from the preparation of the atomic source prior to the entrance in the interferometric zone and to the detection of the atoms at the AI output. The inertial information during these preparation and detection periods is lost. Dead times, for example, strongly mitigate the possibility to realize inertial measurement units (IMUs) based on AIs [19]. In addition, the sequential operation of AIs leads to inertial noise aliasing, which degrades the AI sensitivity in the presence of dead times. This reduces the performance of AIs of potentially high sensitivities [14]. High data rate interferometers using recapture methods have been reported to partially overcome the problem of dead times but at the cost of strong reduction of sensitivity [20]. The inertial noise aliasing in AIs can be alleviated by using auxiliary sensors of large bandwidth [21], but this limits the sensitivity during the dead time period to that of

the auxiliary sensor. Continuous operation (i.e., without dead times) is therefore a key point to benefit from the full potential of atom interferometry.

In this Letter, we report the first continuous operation of a cold-atom inertial sensor. We demonstrate such operation in an AI gyroscope which features a Sagnac area of 11 cm^2, representing a 27-fold increase with respect to previous experiments [22]. The continuous operation improves the short-term sensitivity of the gyroscope, which we illustrate by demonstrating a rotation sensitivity of $100 \text{ nrad/sec}/\sqrt{\text{Hz}}$. Moreover, we show that the continuous operation does not affect the long-term sensitivity potential of AIs and report a stability of 1 nrad/sec after 10^4 sec of integration time.

The principle of the experiment is sketched in Fig. 1. We realize a light-pulse AI using two counterpropagating Raman beams which couple the $|F = 3, m_F = 0\rangle$ and $|F = 4, m_F = 0\rangle$ clock states of Cesium atoms. According to the Sagnac effect [23,24], the rotation sensitivity of the AI is proportional to the area enclosed by the 2 arms. Our AI gyroscope is based on a fountain configuration with four Raman pulses to create a folded geometry thanks to gravity [3]. Similar folded geometries can be obtained in trapped atom interferometers [25]. The four pulse fountain configuration allows us to increase the interferometric area up to 11 cm^2 and leads to zero dc sensitivity to acceleration. The rotation induced phase shift Φ_Ω is given by

$$\Phi_\Omega = \frac{1}{2}\vec{k}_{\text{eff}} \cdot (\vec{g} \times \vec{\Omega})T^3, \qquad (1)$$

where $\vec{k}_{\text{eff}}$ is the two-photon momentum transfer, $\vec{g}$ is the acceleration due to gravity, $\vec{\Omega}$ is the rotation rate, and T is half the interferometric time. Following atom juggling methods initially introduced to measure collisional shifts in fountain clocks [26], we implement a sequence of joint

FIG. 1.   (a) Schematic and operation principle of the continuous cold-atom gyroscope. Continuous measurement is performed with a joint interrogation sequence where the bottom $\pi/2$ pulse is shared between the clouds entering and exiting the interrogation region. (b) Space-time diagram of the four-pulse AI. We introduce a time asymmetry of ΔT to avoid the recombination of parasitic interferometers resulting from the imperfect π pulses. The gyroscope measures rotation rate along the y direction, i.e., perpendicular to the AI area.

interrogation of successive atom clouds as described in Ref. [27]; see Fig. 1(a). Experimentally, the joint operation is obtained by using the same $\pi/2$ Raman pulse for the clouds entering and exiting the AI zone. Thus, the experiment cycle time T_c equals the AI interrogation time $2T$.

Cesium atoms loaded from a 2D magneto-optical trap (MOT) are trapped and cooled in a 3D MOT during 200 msec. We launch 2×10^7 atoms vertically at a speed of 5.0 m/ sec using moving molasses with a (3D) cloud temperature of 1.2 μK. Light pulse interferometry is realized using two phase-locked Raman lasers which couple the Cesium clock states characterized by an hyperfine splitting corresponding to 9.192 GHz. The Raman lasers are sent to the atoms through two optical windows separated by 58 cm, yielding an interrogation time $2T = 800$ msec. We use Raman beams with $1/e^2$ diameter equal to 40 mm and 100 mW of total power. After the MOT and prior to the interrogation, 2×10^6 atoms are prepared in the $|F = 4, m_F = 0\rangle$ state. The AI output signal is determined by the probability of transition from the $F = 4$ to the

$F = 3$ state, which is experimentally realized using fluorescence detection of the two levels after the AI light-pulse sequence.

We lift the degeneracy between the two $\pm\hbar k_{\mathrm{eff}}$ transitions [28] by tilting the Raman beams by an angle of inclination $\theta = 3.81^\circ$ [Fig. 1(a)]. Large area AIs require precise parallelism of the interrogation beams in order for the two paths to recombine within the coherence length of the cold atoms at the interferometer output [29]. We implement a generic protocol to meet the required beam alignment of the Raman beams in the vertical (z) and horizontal (y) directions. For the z direction, we first measure the two beam angles using Doppler spectroscopy, which determines the parallelism with a precision of 20 μrad. We then operate two 3-pulse AI accelerometers at the bottom and top Raman beam positions with an interrogation time of 60 msec to measure the projection of gravity on the beam directions, which allows us to reach a precision of 5 μrad. To adjust the horizontal (y) parallelism, we optimize the contrast of a Ramsey-Bordé AI using the bottom and top Raman beams as described in Ref. [30], and reach a parallelism precision of 200 μrad. With this protocol, we achieve a contrast of 4% in the continuous AI at $2T = 800$ msec, mainly limited by inhomogeneities of the Rabi frequency over the atom cloud extension. For this value of contrast, the AI phase noise due to detection noise amounts to 400 mrad/$\sqrt{\mathrm{Hz}}$ and was estimated with the method described in Ref. [4]. The detection noise level is limited by stray light in the fluorescence detection system and was measured independently without atoms in the interferometer. The limitations associated with joint operation (mainly light shifts and contrast reduction due to scattered light by the MOT) have been described in Ref. [27], together with mitigation strategies.

The AI output signal P is determined by the Earth rotation rate, the vibration noise, and the noninertial noise. We write it as

$$P = P_0 + A \cos\left(\Phi_\Omega + \delta\Phi_{\mathrm{vib}} + \delta\Phi_0\right), \qquad (2)$$

where P_0 is the offset of the interferometric signal, A is the fringe amplitude, Φ_Ω is the rotation phase, $\delta\Phi_{\mathrm{vib}}$ the vibration phase noise, and $\delta\Phi_0$ the noninertial phase noise (e.g., Raman laser phase, light shift). Increasing the AI area necessarily comes at the expense of more sensitivity to the vibration noise, $\delta\Phi_{\mathrm{vib}}$, which has to be reduced to extract the rotation signal, Φ_Ω. The experiment is mounted on a vibration isolation platform to reduce the effect of vibration noise above $\sim$1 Hz to an rms AI phase noise of about 2.5 rad. As the vibration noise spans more than one interferometric fringe, information from additional inertial sensors is necessary to recover the signal.

We further reduce the vibration noise by means of auxiliary sensors which record the acceleration noise of the setup [31]. We mount two commercial accelerometers
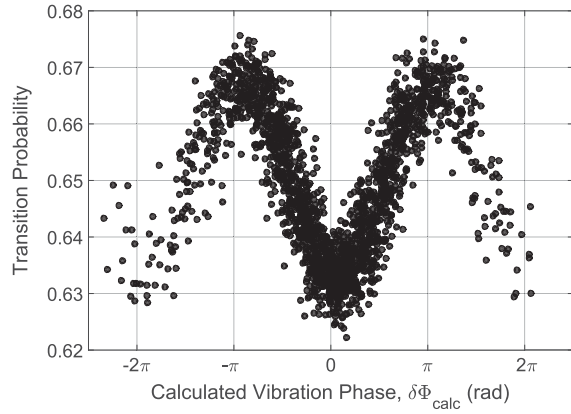
FIG. 2.   Correlation between the AI signal and the vibration phase calculated from the signal of auxiliary accelerometers. The AI interrogation time is $2T = 800$ msec.
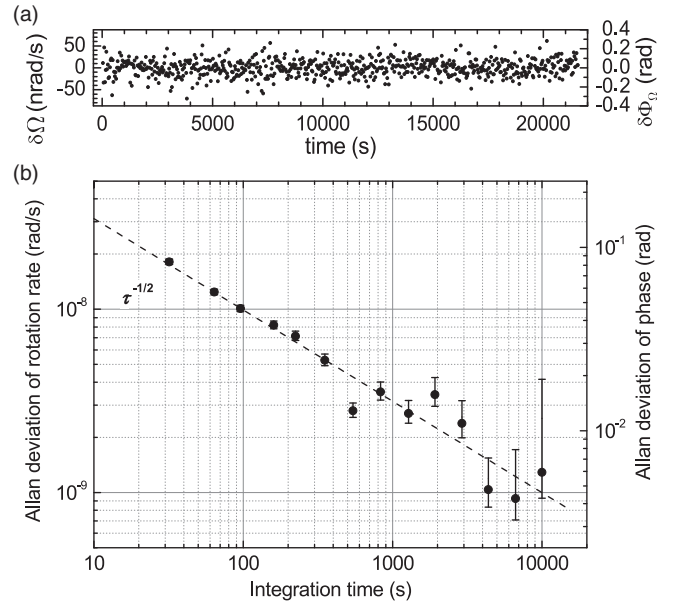

FIG. 3.   (a) Temporal variation of the rotation rate around its mean value. Each point is obtained from the combination of the two phase measurements extracted from correlation fringes (as shown in Fig. 2) involving 20 data points for each of the two opposite Raman wave vectors $+k_{\mathrm{eff}}$ and $-k_{\mathrm{eff}}$. (b) Allan deviation of the gyroscope sensitivity. The dashed line is a guide to the eye illustrating the $\tau^{-1/2}$ scaling. The error bars represent the 68% confidence intervals.

(model Titan from Nanometrics) on the top and bottom of the experimental structure [see Fig. 1(a)], and compute the expected vibration phase $\delta\Phi_{\mathrm{calc}}$ using the four-pulse AI transfer function. Figure 2 shows the correlation between the AI output signal, P, and the phase $\delta\Phi_{\mathrm{calc}}$ calculated from the weighted average of the two accelerometers. As the correlation function is nonlinear, we use the method described in Ref. [31] to extract the rotation rate sensitivity of the interferometer. We divide the total data set in packets of 20 data points and fit a sinusoid to extract the offset phase and hence the rotation rate Ω. This procedure yields a short-term sensitivity of 450 mrad/$\sqrt{\mathrm{Hz}}$, equivalent to rejecting the vibration noise by a factor 5. The rejection efficiency is limited by the detection noise level which currently bounds the short-term sensitivity of the AI.

Figure 3(a) shows an uninterrupted operation of the continuous cold-atom gyroscope over more than 20 000 sec. The Allan deviation of the rotation rate sensitivity is shown in Fig. 3(b). We achieve a short-term sensitivity of 100 nrad/ sec /$\sqrt{\mathrm{Hz}}$, which establishes the best performance to date for cold-atom gyroscopes [22], and represents an improvement of more than 30 compared to previous 4-pulse gyroscopes [3,5]. We compared the operation of the gyroscope in normal and continuous modes and observed a sensitivity improvement of $\simeq 1.4$. This is consistent with the expected value of $[T_c^{(n)}/2T]^{-1/2}$, where $T_c^{(n)} = 2T + T_D$ is the cycle time in normal mode with a dead time $T_D \simeq 0.8$ sec.

The stability of the rotation rate measurement improves as $\tau^{-1/2}$ and reaches 1 nrad/ sec at 10 000 sec of integration time. This represents the state of the art for atomic gyroscopes [32] (see Ref. [24] for a recent review) and a more than tenfold improvement compared to previous cold-atom gyroscopes [22,33]. The long-term stability of our gyroscope is a direct consequence of the large Sagnac area: the AI scale factor in our folded four-pulse geometry scales as T^3 when the instabilities linked to fluctuations of the

atom cloud trajectories and identified as limits in previous experiments [22,33] scale as T. Their impact is thus reduced in our long-T interferometer. We further eliminate the effect of drifts in one-photon light shift originating from drifts of the power ratio of the Raman lasers. This is accomplished by alternating measurements with $\pm k_{\mathrm{eff}}$ momentum transfer and combining the fitted phase values obtained from the 20-points correlation data sets.

To avoid the interference of parasitic interferometers originating from the imperfect $\pi/2$ and π pulses, we introduce a time asymmetry of $\Delta T = 300\ \mu$sec in the Raman pulse sequence [5]; see Fig 1(b). The asymmetry introduces a sensitivity to dc acceleration given by $\Phi_{\mathrm{dc}} = 2k_{\mathrm{eff}}T\Delta T g \sin\theta$. Fluctuations of the angle of inclination of the Raman beams by $\delta\theta$ would result in fluctuations of the AI phase Φ_{dc}. To minimize these fluctuations, we stabilize the vibration isolation platform by measuring the tilt of the experiment and using its signal to compensate the tilt variation via a current-controlled magnetic actuator. We stabilize $\delta\theta$ at the level of 3×10^{-8} rad, ensuring long-term stabilization of Φ_{dc} below 0.3 nrad/ sec after 2000 sec of integration. Moreover, we alternated measurements with $\pm\Delta T$ and did not observe any effect on the rotation signal, as expected. The tilt in the y direction was measured to drift by less than 10 μrad, yielding a negligible phase drift due to a different projection of the rotation vector on the interferometer area.

Our results represent record inertial sensitivities in a Sagnac AI. We emphasize that such performances were obtained, for the first time, without loss of information on the inertial signal thanks to the joint operation of the interferometer. In our setup, the sensitivity is currently limited by the detection noise, yielding a $\tau^{-1/2}$ scaling of the rotation stability. Improving the contrast of our AI (e.g., with more powerful and larger Raman beams) and reducing the stray light in our current detection system would result in a lower detection noise limit. In that case, the continuous operation would offer the possibility to efficiently average the vibration noise as τ^{-1} as a result of noise correlations between successive measurements. Such scaling of the sensitivity has been demonstrated in clock configurations to average the local oscillator noise [27,34]. The continuous operation which we demonstrated here will then enable us to quickly reach the quantum projection noise (or Heisenberg) limit in large area AIs. Assuming a vibration noise averaging as τ^{-1}, a quantum projection noise limited detection with 10^6 atoms and a 20% interferometer contrast, a rotation sensitivity below 1×10^{-10} rad/sec in few 100 sec is thus accessible with our setup.

If we assume negligible detection noise, observing the τ^{-1} scaling would require to operate the AI in its linear region, i.e., around midfringe. Otherwise, the loss of inertial sensitivity, which occurs when approaching the top and bottom of the fringe, prevents us from observing the τ^{-1} scaling (see Fig. S1 in the Supplemental Material [35] for a simulation). Midfringe operation can, for example, be achieved by a real time compensation of vibrations with a feedback to the Raman laser phase [21].

The sensitivity reached by our instrument allows us to foresee applications in geodesy and geophysics. High rotation rate sensitivity combined with the large bandwidth obtained by continuous operation and the multiple-joint technique [27] would allow, for instance, the detection of the rotational signatures of seismic signals that cover a wide range of rotation rates from 10^{-14} rad/sec to 1 rad/sec with typical signal frequencies in the range of few mHz to tens of Hz [36]. Moreover, signals due to Earth tides, polar motion and ocean loading could be accessible with our device.

The continuous operation which we demonstrated here paves the way to inertial navigation based on AIs, by fully exploiting the sensitivity and long-term stability of atomic sensors without loss of information [19]. Finally, the continuous operation will benefit fundamental physics experiments with AIs, in particular, when looking for time varying signals such as in gravitational wave detection [10,11].

[*]remi.geiger@obspm.fr
[†]arnaud.landragin@obspm.fr

[1] R. Bouchendira, P. Cladé, S. Guellati-Khélifa, F. Nez, and F. Biraben, Phys. Rev. Lett. **106**, 080801 (2011).

[2] G. Rosi, F. Sorrentino, L. Cacciapuoti, M. Prevedelli, and G. M. Tino, Nature (London) **510**, 518 (2014).

[3] B. Canuel, F. Leduc, D. Holleville, A. Gauguet, J. Fils, A. Virdis, A. Clairon, N. Dimarcq, C. J. Bordé, A. Landragin, and P. Bouyer, Phys. Rev. Lett. **97**, 010402 (2006).

[4] R. Geiger, V. Menoret, G. Stern, N. Zahzam, P. Cheinet, B. Battelier, A. Villing, F. Moron, M. Lours, Y. Bidel, A. Bresson, A. Landragin, and P. Bouyer, Nat. Commun. **2**, 474 (2011).

[5] J. K. Stockton, K. Takase, and M. A. Kasevich, Phys. Rev. Lett. **107**, 133001 (2011).

[6] P. Gillot, O. Francis, A. Landragin, F. P. D. Santos, and S. Merlet, Metrologia **51**, L15 (2014).

[7] R. Geiger et al., in Proceedings of the 50th Rencontres de Moriond, edited by E. Augé, J. Dumarchez, and J. Trân Thanh Vân (ARISF, La Thuile, Italy, 2015).

[8] C. Freier, M. Hauth, V. Schkolnik, B. Leykauf, M. Schilling, H. Wziontek, H.-G. Scherneck, J. Müller, and A. Peters, arXiv:1512.05660.

[9] G. Rosi, L. Cacciapuoti, F. Sorrentino, M. Menchetti, M. Prevedelli, and G. M. Tino, Phys. Rev. Lett. **114**, 013001 (2015).

[10] S. Dimopoulos, P. W. Graham, J. M. Hogan, M. A. Kasevich, and S. Rajendran, Phys. Rev. D **78**, 122002 (2008).

[11] W. Chaibi, R. Geiger, B. Canuel, A. Bertoldi, A. Landragin, and P. Bouyer, Phys. Rev. D **93**, 021101 (2016).

[12] P. Cladé, S. Guellati-Khélifa, F. Nez, and F. Biraben, Phys. Rev. Lett. **102**, 240402 (2009).

[13] S.-w. Chiow, T. Kovachy, H.-C. Chien, and M. A. Kasevich, Phys. Rev. Lett. **107**, 130403 (2011).

[14] S. M. Dickerson, J. M. Hogan, A. Sugarbaker, D. M. S. Johnson, and M. A. Kasevich, Phys. Rev. Lett. **111**, 083001 (2013).

[15] H. Müntinga et al., Phys. Rev. Lett. **110**, 093602 (2013).

[16] J. E. Debs, P. A. Altin, T. H. Barter, D. Döring, G. R. Dennis, G. McDonald, R. P. Anderson, J. D. Close, and N. P. Robins, Phys. Rev. A **84**, 033610 (2011).

[17] I. D. Leroux, M. H. Schleier-Smith, and V. Vuletić, Phys. Rev. Lett. **104**, 073602 (2010).

[18] O. Hosten, N. J. Engelsen, R. Krishnakumar, and M. A. Kasevich, Nature (London) **529**, 505 (2016).

[19] C. Jekeli, Navigation **52**, 1 (2005).

[20] H. J. McGuinness, A. V. Rakholia, and G. W. Biedermann, Appl. Phys. Lett. **100**, 011106 (2012).

[21] J. Lautier, L. Volodimer, T. Hardin, S. Merlet, M. Lours, F. Pereira Dos Santos, and A. Landragin, Appl. Phys. Lett. **105,** 144102 (2014).

[22] P. Berg, S. Abend, G. Tackmann, C. Schubert, E. Giese, W. P. Schleich, F. A. Narducci, W. Ertmer, and E. M. Rasel, Phys. Rev. Lett. **114,** 063002 (2015).

[23] G. Sagnac, C.R. Acad. Sci. (Paris) **157,** 708 (1913).

[24] B. Barrett, R. Geiger, I. Dutta, M. Meunier, B. Canuel, A. Gauguet, P. Bouyer, and A. Landragin, C.R. Phys. **15,** 875 (2014).

[25] S. Wu, E. Su, and M. Prentiss, Phys. Rev. Lett. **99,** 173201 (2007).

[26] R. Legere and K. Gibble, Phys. Rev. Lett. **81,** 5780 (1998).

[27] M. Meunier, I. Dutta, R. Geiger, C. Guerlin, C. L. Garrido Alzar, and A. Landragin, Phys. Rev. A **90,** 063633 (2014).

[28] T. Lévèque, A. Gauguet, F. Michaud, F. Pereira Dos Santos, and A. Landragin, Phys. Rev. Lett. **103,** 080405 (2009).

[29] J. R. Kellogg, N. Yu, J. M. Kohel, R. J. Thompson, D. C. Aveline, and L. Maleki, J. Mod. Opt. **54,** 2533 (2007).

[30] G. Tackmann, P. Berg, C. Schubert, S. Abend, M. Gilowski, W. Ertmer, and E. M. Rasel, New J. Phys. **14,** 015002 (2012).

[31] S. Merlet, J. Le Gouët, Q. Bodart, A. Clairon, A. Landragin, F. Pereira Dos Santos, and P. Rouchon, Metrologia **46,** 87 (2009).

[32] D. S. Durfee, Y. K. Shaham, and M. A. Kasevich, Phys. Rev. Lett. **97,** 240801 (2006).

[33] A. Gauguet, B. Canuel, T. Lévèque, W. Chaibi, and A. Landragin, Phys. Rev. A **80,** 063604 (2009).

[34] G. W. Biedermann, K. Takase, X. Wu, L. Deslauriers, S. Roy, and M. A. Kasevich, Phys. Rev. Lett. **111,** 170802 (2013).

[35] See Supplemental Material at http://link.aps.org/supplemental/10.1103/PhysRevLett.116.183003 for a simulation showing the breakdown of the τ^{-1} scaling when operating the AI beyond midfringe.

[36] K. U. Schreiber and J.-P. R. Wells, Rev. Sci. Instrum. **84,** 041101 (2013).